6-11-2013

Frequency-selective surface coupled metal-oxide-metal diodes

Edward C. Kinzel

Robert Laurent Brown

James Chris Ginn

Brian A. Lail

Brian A. Slovick

See next page for additional authors

Authors

Edward C. Kinzel, Robert Laurent Brown, James Chris Ginn, Brian A. Lail, Brian A. Slovick, and Glenn D. Boreman

Frequency-Selective Surface Coupled Metal-Oxide-Metal Diodes

Edward C. Kinzel*[a], Robert L. Brown[b], James C. Ginn[c], Brian A. Lail[d], Brian A. Slovick[e], Glenn D. Boreman[f]

[a]Missouri University of Science & Technology, 400 W. 13th St., Rolla, MO, USA 65409; [b]Northwestern, 2145 Sheridan Rd., Evanston, IL USA 60208; [c]Plasmonics Inc., 4000 Central Florida Blvd., Orlando FL USA 32816; [d]Florida Institute of Technology, 150 W. University Blvd., FL USA 32901; [e]SRI International, 333 Ravenswood Ave., Menlo Park, CA USA 94025; [f]University of North Carolina at Charlotte, 9201 University City Blvd, Charlotte, NC USA 28223

ABSTRACT

Metal-Oxide-Metal diodes offer the possibility of directly rectifying infrared radiation. To be effective for sensing or energy harvesting they must be coupled to an antenna which produces intense fields at the diode. While antennas significantly increase the effective capture area of the MOM diode, it is still limited and maximizing the captured energy is still a challenging goal. In this work we investigate integrating MOM diodes with a slot antenna Frequency Selective Surface (FSS). This maximizes the electromagnetic capture area while minimizing the transmission line length which helps reduce losses because metal losses are much lower at DC than at infrared frequencies. Our design takes advantage of a single self-aligned patterning step using shadow evaporation. The structure is optimized at 10.6 μm to have less than 2% reflection (polarization sensitive) and simulations predict that 70% of the incident energy is dissipated into the oxide layer. Initial experimental results fabricated with e-beam lithography are presented and the diode coupled FSS is shown to produce a polarization sensitive unbiased DC short circuit current. This work is promising for both infrared sensing and imaging as well as direct conversion of thermal energy.

Keywords: Frequency selective surface, metal-oxide-metal diode, shadow evaporation, infrared, rectenna

1. INTRODUCTION

Antenna coupled Metal-Oxide-Metal (MOM) diodes have generated significant interest for use in uncooled infrared sensing [1-3] as well as direct energy conversion for solar/thermal harvesting [4]. MOM diodes have been studied at THz and infrared frequencies since the late 1960s [5]. They are attractive for rectification and frequency mixing because of their very fast response times [4] and compatibility with standard CMOS processing [1]. Modern nanofabrication techniques have facilitated their implementation with high-frequency antennas to produce working devices at infrared and optical wavelengths [6].

At radio frequencies, rectennas have achieved up to 90% power transfer efficiency [7]. However, there are obstacles to realizing this performance at infrared/optical wavelengths. One of the most significant is the economic fabrication of nanoscale structures. These feature sizes are dictated by the wavelength of light at optical/infrared frequencies as well as the RC time constant of the diode [5-6] and the optical properties of metals at infrared/optical wavelengths [8]. For example, Bean et al. [2] predicted that a 75×75 nm area overlap or smaller would be required for a diode system similar to what is studied this paper not to be cutoff at 28.3 THz. These feature sizes are possible with e-beam lithography (EBL), however, this is not suitable for economic large scale production required for either focal plane arrays (FPA) or for energy harvesting applications. Roll-to-roll nanoimprint lithography (R2RNIL) appears to be a way forward for patterning relatively large areas with the feature sizes required for antenna coupled diodes [9]. The shadow evaporation technique, proposed by Dolan [10] and developed for antenna coupled MOM diodes by Bean et al. [1], allows patterning antenna-coupled-diodes with a single lithography step. This will be advantageous for use with R2RNIL because it removes the need for nanoscale alignment between layers.

New antenna/diode designs at optical and infrared frequencies are in need of development. Both sensing and energy harvesting applications require efficiently capturing radiation from an area larger than that of a single antenna ($\lambda^2/4\pi$ for the lossless isotropic case). This requires the efficient integration of multiple antennas and can be accomplished two ways. Several antennas can be connected to a single diode using transmission lines to form a phased array [3]. On the other hand, each antenna can be connected to its own transducer, which are in turn connected at DC [12]. Increased

*kinzele@mst.edu; phone 1 573 341-7254;

Infrared Technology and Applications XXXIX, edited by Bjørn F. Andresen, Gabor F. Fulop, Charles M. Hanson, Paul R. Norton, Proc. of SPIE Vol. 8704, 87041C · © 2013 SPIE
CCC code: 0277-786X/13/$18 · doi: 10.1117/12.2014777

ohmic losses and greater field penetration are fundamental to metals at optical and infrared wavelengths. For example, Mandviwala et al. [11] found the 1/e propagation length for standard RF style waveguides to be less than 14 μm at λ=10.6 μm. It is more efficient to integrate the diode with the antenna and then transmit and combine the rectified energy at DC.

Similar to rectennas, Frequency-Selective Surfaces (FSS) were originally developed at microwave frequencies [13], but have been scaled to infrared [14] as well as optical wavelengths. A FSS consists of a periodically arranged array of resonant metallic antenna elements on a dielectric surface. They allow a surface's transmitance, reflectance, and absorptance to be engineered as a function of wavelength, polarization, and angle of incidence. The behavior of the FSS is a function of the geometry of the resonant elements, the array spacing, and the materials making up the elements and the dielectric surface. When matched to the incident radiation they have been demonstrated capable of almost unity absorptance, corresponding to near unity emittance from Kirchhoff's law [15]. However, in this case the infrared frequency currents are largely dissipated in the metallic elements of the structure.

In this paper we demonstrate a slot-antenna-based FSS with integrated MOM diodes. This has several advantages for both sensing and energy harvesting. The slot-based design helps to limit the high-frequency currents to the diode. It also makes use of shadow evaporation for a single patterning step which facilitates scaling the design to higher volume fabrication. We optimize the structure for polarized radiation at 10.6 μm by impedance matching the FSS to the diode and the entire structure to free space. This wavelength was selected for testing with a CO_2 laser and is near the peak thermal emission from objects at room temperature, however, the design could easily be scaled to shorter wavelengths for energy harvesting. Under linear polarized illumination, the simulation predicts that the FSS has near-unity absorptance with up to 70% of the power dissipated in the oxide layer. This corresponds to the maximum voltage across the diode which is rectified to produce a DC current. For energy harvesting applications the FSS can be pared with a second emitting FSS that only radiates the correct polarization and at the optimal wavelength [15-16]. The paper presents the design of the diode coupled FSS. It is studied and optimized numerically. We present initial fabrication results which demonstrate the viability of the design. Finally, we discus these results and present suggestions for future work.

2. GEOMETRY AND FABRICATION

Figure 1a shows the geometry of the diode coupled FSS. Each unit cell is 3.75×3.50 μm. The FSS consists of a densely packed slot antenna array separated from an optically thick aluminum ground plane by a benzocyclobutene (BCB) standoff. At the center of each slot antenna is a shadow-evaporated diode. The slot antenna is defined in a metal plane that is divided for DC isolation. The simulated geometry modeled to reflect SEM images of past devices. The thickness of the aluminum and platinum layers are 30 nm and 25 nm, respectively. The oxide is 10 Å thick and only modeled in the diode gap, following the approach of [3], and shown in the inset of Fig. 1. Simulations show that the high-frequency electromagnetic performance of the FSS is not affected by including the thin oxide layer in other regions and neglecting it simplifies the model, improving the speed during optimization of the structure. Figure 1b shows the dimensions of the EBL pattern used to define the antenna/diode structure.

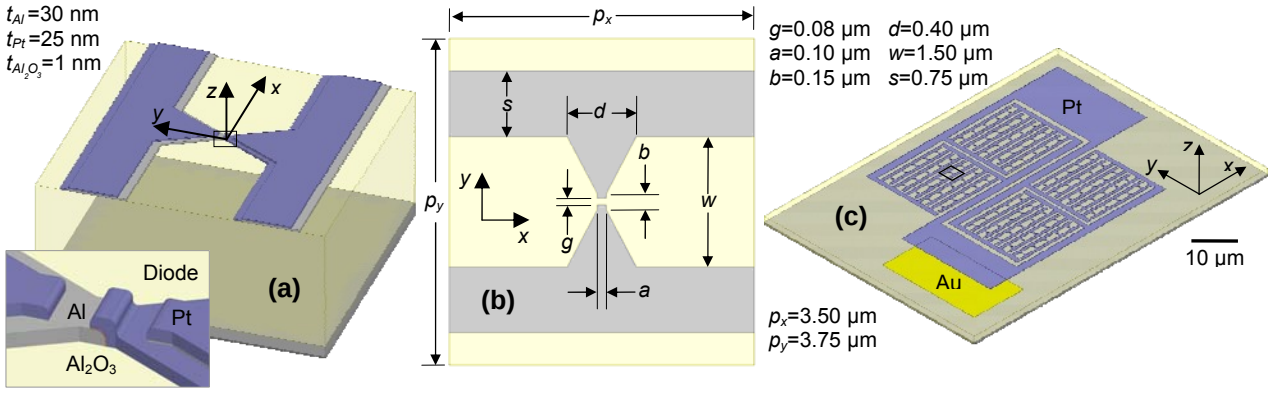

Figure 1: (a) Unit cell geometry (b) e-beam lithography layout used for defining pattern, and (c) device assembled from 100 unit cells .in parallel

The unit cell in Figs. 1a and 1b can be assembled to form a functional device, such as is shown in Fig. 1c. The DC wires are continuous and connect each slot antenna/diode in parallel to bond pads. The net current flow at DC is from the aluminum side of the diode to the platinum. Because the aluminum contact is almost completely covered by platinum it is difficult to probe directly. A gold contact can be deposited prior to patterning the slot antenna/diodes. Gold is attractive because it will not oxidize during the subsequent processing/patterning of the diodes. Because the contact is relatively large it does not require patterning with EBL or precise alignment to the finely patterned structure. The feed structure does not capture a significant amount of incident light itself, however making lead lines too small will raise the DC resistance. This produces a tradeoff between the DC and high-frequency performance of the device which should be further optimized.

The unit cell in Fig. 1 is fabricated following the shadow-evaporation approach described in [1,2] illustrated in Fig. 2. The FSS and electrical lead geometry were patterned on top of a 1.6 μm thick BCB standoff above an optically thick aluminum ground plane using the exposure pattern shown in Fig. 1b. E-beam lithography (EBL) is used to pattern a bi-layer poly(methyl methacrylate) (PMMA)/MMA resist stack. The underlying MMA is more sensitive to the exposing electron beam than the PMMA which results in a undercut profile after development using MIBK:IPA (1:3). Following development the sample is placed in an O_2 plasma barrel etcher to remove any undesired resist. Proper selection of the pattern geometry and electron beam dosage results in an air-bridge of PMMA in the gap of the antenna. E-beam evaporation is used to deposit Al with the sample rotated a small angle from the normal. The sample is then exposed to in situ to 50 mTorr partial pressure O_2 for 30 minutes which allows a 10-20 Å native oxide layer to form over the Al. Following the oxidation Pt is deposited at an opposing angle to the first deposition. Provided that there is sufficient undercutting of the MMA, the offset is determined by the deposition angle. The thickness of the oxidation is critical to the process and was studied in detail by Bean et al. in [2].

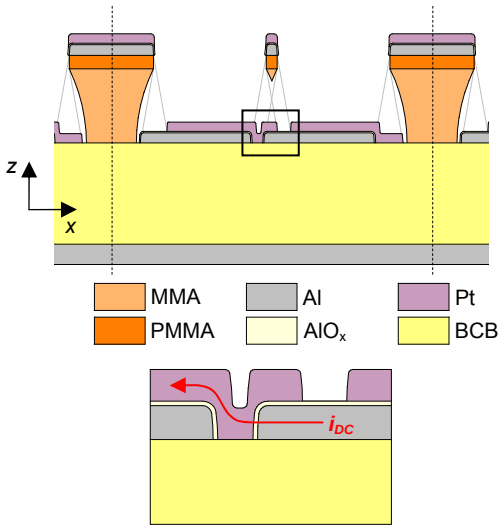

Figure 2: Diode fabrication using shadow-evaporation and lift-off.

Figure 3 shows SEM images of the fabricated device. These were taken after testing the devices to prevent charging and damaging the diodes by the SEM. The globs of material in Fig. 3a are silver paste. This initial experimental device did not use the gold contacts shown in Fig. 1c so must be probed through the platinum. This assumes that there are at least some pinholes in the oxide connecting the platinum layer to the aluminum layer. Because of the large area of the feed structure relative to diode there is a greater chance that the pinholes will occur outside the active diode region, but the reliance on pinholes significantly limits the performance of the device. Figures 3b and 3c show closer images of the same diode-coupled FSS structure. At least some of the diodes did not completely lift out and contribute to the shorting out of the device. The figures show that there is nontrivial surface roughness in the FSS. This is not a factor electromagnetically, however, within the diode region it contributes to a greater chance of pinholes.

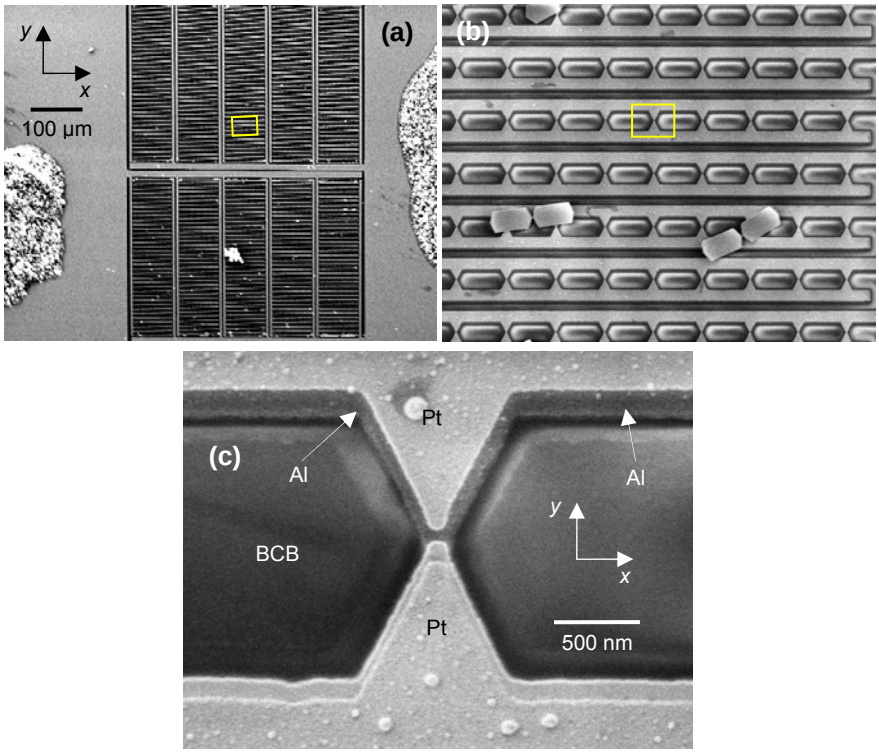

Figure 3. SEM images of fabricated MOM diode coupled FSS. (a) Image of entire array consisting of 16,800 diode-coupled elements in an active area less than 0.325 mm^2. (b) Closer image of the array showing several pieces of metal coated photoresist that became attached to the sample after lift-off and (c) diode of working device.

3. ELECTROMAGNETIC AND THERMAL SIMULATION

The diode-coupled FSS was modeled as an infinite array and excited with a Floquet port in HFSS (ANSYS Inc.) The geometry of the FSS was optimized to provide minimal reflection under normally incident 28.3 THz (λ_0=10.6 µm) illumination while maximizing the fraction of power dissipated in the diode oxide. Frequency dependent material properties for Al, Pt, BCB, and Al_2O_3 were obtained from spectrographic ellipsometry (IR-VASE, J.A. Woollam) and are shown in Fig. 4. The native AlO_x oxide is modeled using the properties of Al_2O_3 which has a broad phonon resonance at ~12 µm. At λ=10.6 µm the properties used in the simulation for Al_2O_3 are $\varepsilon'+j\varepsilon''=-0.41+j0.11$. Also of note are absorption peaks in BCB centered at 9.5 and 12 µm, however, at λ_0=10.6 µm its properties are $\varepsilon'+j\varepsilon''=2.43+j0.07$. In the structure, the incident field couples to the slot antenna resonance which induces current through the diode. This resonance can be tuned by adjusting the feature sizes and the standoff. Figure 5 shows the fields in the unit cell when it is exposed to λ=10.6 µm *y*-polarized radiation. The simulation predicts that the electric field is concentrated 2000× across the diode.

Figure 6 shows the simulated reflectance of the FSS for *x*- and *y*-polarizations. At the design wavelength the reflectance is less than 2% for *x*-polarized light and 90% for *x*-polarized illumination. Because of the groundplane there is no transmission through the structure. More than 70% of the power is dissipated in the oxide due to the extreme field concentration. This shows that the collective structure is well matched to free-space while within the unit cell there is good slot/diode impedance matching. Off-resonance there is less of a match to the oxide and power is instead dissipated in the BCB and metal components of the structure.

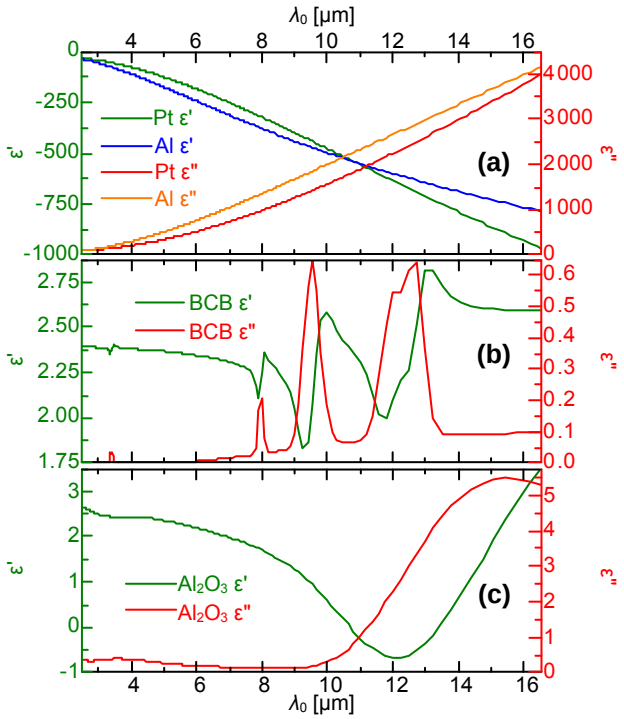

Figure 4: Optical properties used in HFSS model obtained from spectrographic ellipsometry. (a) Metals, (b) BCB, and (c) Al_2O_3.

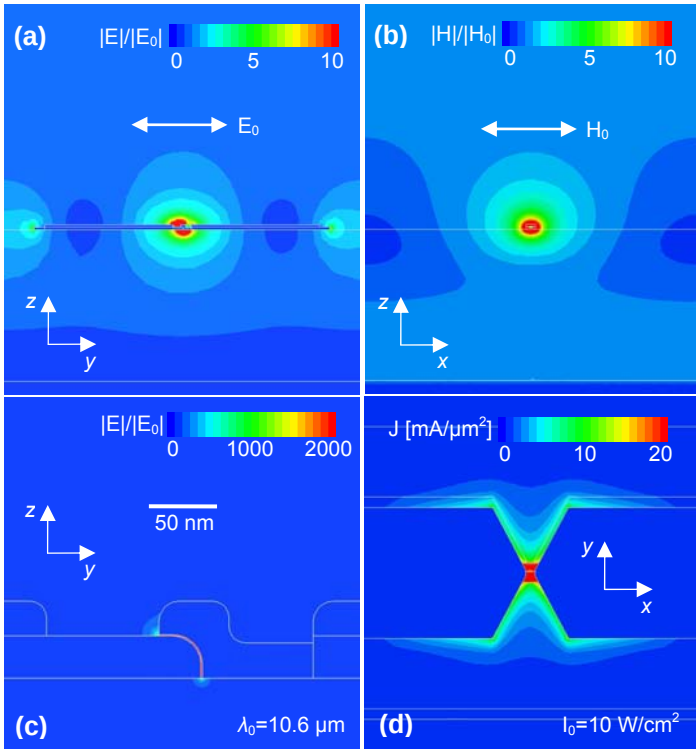

Figure 5: Electromagnetic resonance inducing high-frequency current through diode under y-polarized 10.6 μm normal illumination. (a) E-plane (b) H-plane (c) close up of E-field on diode and (c) current density on xy plane.

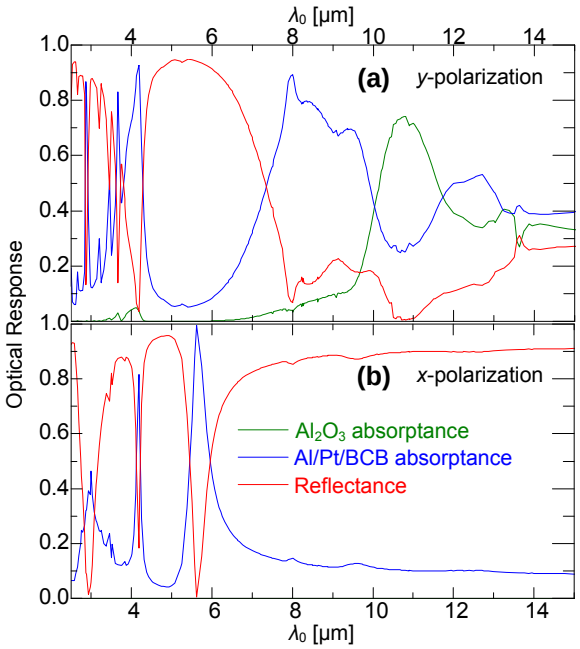

Figure 6: HFSS simulation of FSS response under illumination with (a) x-polarized and (b) y-polarized light.

Slovick et al. [3] showed that the power dissipated in the oxide is proportionate to signal (short circuit current) generated by the diode. This is because power dissipated in the oxide scales with the voltage across the diode which determines the rectified current. The first nonzero term in a power series expansion of the rectified current is [3]

$$I_r = \frac{1}{4}\frac{d^2 I}{dV^2}\bigg|_{V=V_b} V_0^2 \tag{1}$$

where V_b is the bias voltage and V_0 is the voltage across the diode. The voltage across the diode is evaluated numerically using a line integral of the electric field and plotted in Fig. 7 for an incident intensity of 10 W/cm^2. Because of the aspect ratio of the diode this is close to constant over its area. The voltage differs slightly from the power dissipation due to frequency dependent conductivity of the oxide. It is important to note that this model of the FSS is limited to electromagnetic analysis. Therefore it is fundamentally linear and does not account for the tunneling effects in the diode.

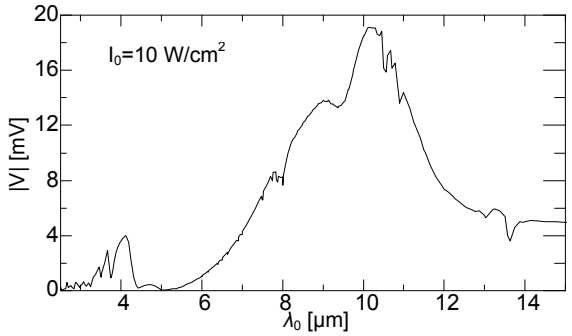

Figure 7. HFSS simulation of voltage across the diode for *x*-polarized radiation.

It is worth considering the thermal response because it can potentially affect the performance of the device and in the absence of a rectifying diode could be used to detect incident radiation. Figures 8a and b shows the steady state temperature under *y*- and *x*- polarized I_0=10 W/cm^2, λ=10.6 μm illumination. This was calculated using ANSYS V14 based on the electromagnetic absorption predicted by HFSS. Convection and radiation were neglected on the top surface, while the bottom surface was held at a fixed temperature because of its high thermal conductivity and contact with silicon. The results showed a 0.82°C maximum temperature rise for *y*-polarized illumination, with minimal thermal

change under cross-polarized illumination. Due to rapid thermal diffusion along the metal leads, minimal temperature variance would be anticipated over the entire structure. This self-quenching behavior, leads to a rise time of lest than 25 μs. It is important to note, that as part of this study similar thermal models of the MOM-diode coupled phased antenna arrays, presented in [3] were studied. These thermal simulations could not predict the far-field radiation patterns experimentally demonstrated for the phased arrays and lend credence to the rectification arguments for antenna coupled MOM-diode [1-5].

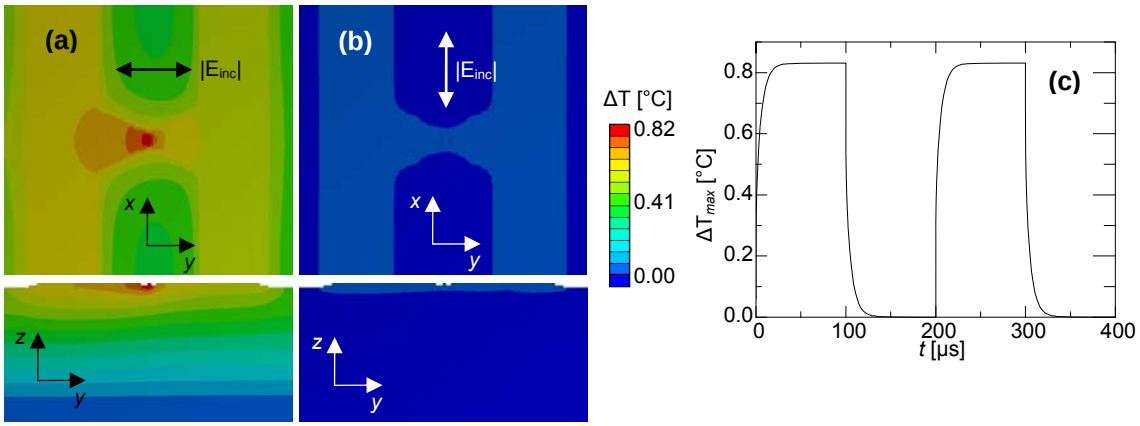

Figure 8: Thermal response of the FSS unit cell: Steady state under normal illumination with (a) *x*-polarized and (b) *y*-polarized 10 W/cm^2, 10.6 μm light. (c) Transient response under *x*-polarized illumination chopped at 10 kHz.

4. CHARACTERIZATION AND MEASUREMENT

The large number of diode-coupled FSS elements were patterned to provide a sufficient area for FTIR measurements. Figure 9 shows experimental reflectance spectra for the device in Fig. 3 collected using a Perkin Elmer micro-FTIR spectrometer. There is qualitative agreement between the experimental and simulated spectra. This shows qualitative agreement with the results predicted by simulation in Fig. 6. At the design wavelength the measurement shows a reflectance of 5% and 80% under *y*- and *x*-polarization, respectively. The discrepancy from simulation can be attributed to some of the light being reflected specularly from the feed structure as well as errors in modeling the native oxide's optical properties and exact diode geometry. These considerations are of utmost significance to the operation of the diode but are difficult to resolve directly with FTIR.

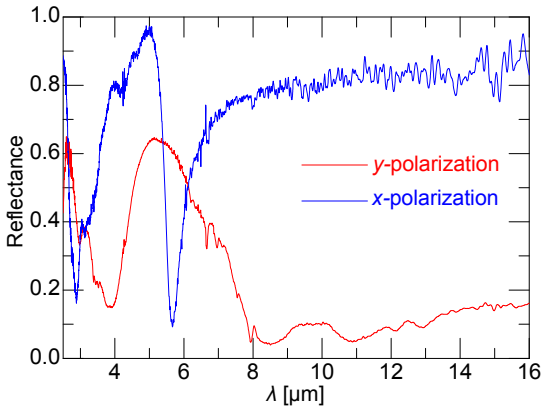

Figure 9. FTIR measured reflectance.

Figure 10 shows the measured DC parameters for the fabricated device. It behaves as if it was a 125 Ω resistor with limited nonlinearity (8.95 μA/V^2 at 0 bias). This is much less resistance (220 kΩ in [2]) as well as lower nonlinearity than other fabricated devices using similar diode dimensions reported in literature (3 orders of magnitude lower curvature than [17]). We attribute this to at least some of the diodes being shorted out which as previously mentioned is a necessary condition to probe the Al layer.

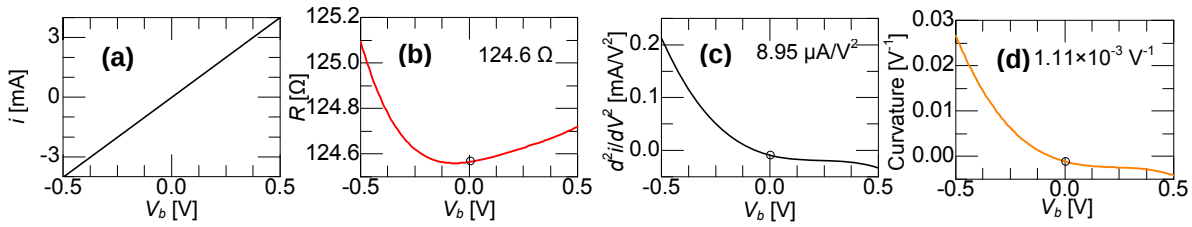

Figure 10. MOM diode coupled FSS DC response. (a) measured *iv* curve, (b) resistance, (c) non-linearity and (d) curvature.

Despite fabrication irregularities, the device does still show some nonlinearity at 0 bias. Fig. 11 shows the short-circuit response of the device when it is exposed to a polarized CO_2 laser beam. The intensity of the incident beam was ~10 W/cm^2. This beam was chopped and the device shown in Fig. 2 was connected to a lock-in amplifier (LIA). Part of the incident beam was split off and the output of the lock-in amplifier is normalized to the incident beam power. During the experiment the polarization of the incident beam is rotated with a half-wave plate. The figure shows the polarization dependence of the response indicating that the device is functioning despite some unit cells being shorted out.

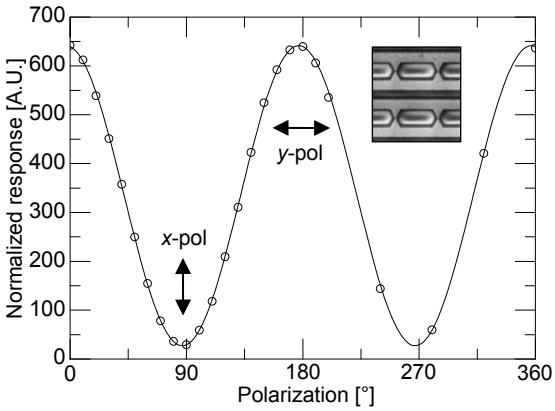

Figure 11. Short circuit response showing polarization dependence.

Future measurements should focus on the biasing the device and measuring the current under different loads. The ultimate goal should be to identify the efficiency under different intensities and at different wavelengths. Of particular interest would be comparing the response of the device at λ=9.3 μm illumination as opposed to λ=10.6 μm to determine the effect of exciting the phonon mode in the oxide.

The true diode impedance will be a slight function of the magnitude of the voltage the structure generates across it. That is the tunneling current will generate an additional resistive component which may effect the matching between the diode, the FSS, and free-space. The true diode impedance at the operational frequency is very challenging to measure experimentally. This structure can provide the ability to indirectly infer the impedance from the reflectance spectra. Although not explored here, incorporating the slot antennas as an inductive element changes the RC diode system to an RLC system. This makes the structure resonant at a given frequency as opposed to cutoff at high frequencies and may relieve some of the size constraints on the diode.

5. CONCLUSION

We have designed, fabricated, and measured a diode coupled FSS. While the fabrication process still requires refinement, agreement between simulation and initial results is promising and demonstrates that a FSS can be well matched to diodes and to free-space. This design was developed for fabrication using self-aligned shadow evaporation. Despite the shorting out of the diodes the device was able to resolve the polarization of an incident laser beam by measuring the short circuit response of the device. The diode-coupled FSS has potential for thermal imaging and can be scaled to shorter wavelengths for energy harvesting. The ability to achieve high field concentrations in a well confined volume may be useful to other sensing applications. General process engineering improvements to avoid shorting out the

diodes should be studied in addition to using a gold (or other inert metal) contact to directly probe the aluminum side of the diode. Different combination of metal/native oxide/metal systems should also be investigated.

REFERENCES

[1] Bean, J.A., Tiwari,, B., Bernstein, G.H., Fay, P., and Porod, W., "Thermal infrared detection using dipole antenna-coupled metal-oxide-metal diodes," J. Vac. Sci. Technol. B 27(1), 11-14 (2009).

[2] Bean, J.A., Weeks, A., and Boreman, G.D., "Performance Optimization of Antenna-Coupled Al/AlOx/Pt Tunnel Diode Infrared Detectors," IEEE J. of Quant. Elect. 47(1), 126-135 (2011).

[3] Slovick, B.A. Bean, J.A. Krenz, P.M. and Boreman, G.D., "Directional control of infrared antenna-coupled tunnel diodes," Opt. Exp. 18(20), 20960-20967 (2010).

[4] Grover, S. and Moddel, G., "Applicability of Metal/Insulator/Metal (MIM) Diodes to Solar Rectennas," IEEE J. of Photovoltaics 1(1), 78-82 (2011).

[5] Sanchez, A., Davis, C.F., Liu, K.C., and Javan, A., "The MOM tunneling diode: Theoretical estimate of its performance at microwave and infrared frequencies," J. Appl. Phys. 49(10), 5270-5276 (1978)

[6] Fumeaux, C., Alda, J., and Boreman, G., "Lithographic antennas at visible frequencies," Opt. Lett. 24(22), 1629-1631 (1999).

[7] Brown, W.C., "Optimization of the efficiency and other properties of the rectenna element," Proc. IEEE-MTT-S Int. Microw. Syp., 142-144 (1976).

[8] Novotny, L., "Effective Wavelength Scaling for Optical Antennas," Phys. Rev. Lett. 98(26), 266802 (2007).

[9] Ahn, S.H., and Guo, L.J., "Large-Area Roll-to-Roll and Roll-to-Plate Nanoimprint Lithography: A Step toward High-Throughput Application of Continuous Nanoimprinting," ACS Nano 3(8), 2304-2310 (2009).

[10] Dolan, G.J., "Offset masks for liftoff photoprocessing," Appl. Phys. Lett. 31(5), 337-339 (1977).

[11] Mandviwala, T.A., Lail, B.A., and Boreman, G.D., "Characterization of Microstrip Transmission Lines at IR Frequencies – Modeling Fabrication and Measurement," Microwave and Opt. Tech. Lett. 50(5), 1232-1237 (2008),

[12] Gonzalez, F.J., Ilic, B., Alda, J., and Boreman, G.D., "Antenna-Coupled Infrared Detectors for Imaging Applications," IEEE J. of Sel. Top. in Quant. Elect. 11(1), 117-120 (2005)

[13] Munk, B.A., [Frequency Selective Surfaces, Theory and Design] Wiley, New York, 2000.

[14] Rhoads, C.M., Damon, E.K., and Munk, B.A., "Mid-infrared filters using conducting elements," Appl. Opt. 21(15), 2814-2816 (1982).

[15] Liu, X., Tyler, T., Starr, T., Starr, A.F., Jokerst, N.M., and Padilla, W.J., "Taming the Blackbody with Infrared Metamaterials as Selective Thermal Emitters," Phys. Rev. Lett. 107(4) 045901 (2011)

[16] Ginn, J., Shelton, D., Krenz, P., Lail, B. and Boreman, G., "Polarized infrared emission using frequency selective surfaces," Opt. Exp. 18(5), 4557-4563 (2010).

[17] Esfandiari, P., Bernstein, G., Fay, P., Porod, W., Rakos, B., Zarandy, A., Berland, B., Boloni, L., Boreman, G., Lail, B. Monacelli, B., and Weeks A., "Tunable Antenna-Coupled Metal-Oxide-Metal (MOM) Uncooled IR Detector," Proc. SPIE 5783, 470-482 (2005)